Generalized PEEC Model for Conductor–Dielectric Problems With Radiation Effect

Yang Jiang, Yuhang Dou, *Student Member, IEEE*, and Ke-Li Wu, *Fellow, IEEE*

***Abstract*— In this article, a passive full-wave partial element equivalent circuit (PEEC) model is formulated for modeling electromagnetic (EM) problems with finite dielectrics. The proposed PEEC model is a substantial extension of the generalized PEEC model for problems of multiple conductors in free space. The proposed generalized PEEC model reflects the physical radiation mechanism of an EM problem with finite dielectrics. The radiation effects, both from conductors and dielectrics, are incorporated in real-valued frequency-dependent inductances and resistances, while capacitances remain to be frequency invariant. Consequently, the resultant circuit model of the proposed PEEC model is numerically verified to be more passive than the existing PEEC models. The minor passivity violation can be amended without altering the circuit configuration. To model a dielectric with the irregular-shaped surface, a triangular meshing scheme with Rao–Wilton–Glisson (RWG) basis is used. The generalized PEEC model provides a passive circuit model for both the frequency- and time-domain modeling of an EM problem with finite dielectrics. The passivity and accuracy of the generalized PEEC model are validated by an low temperature co-fired ceramic (LTCC) multilayer filter module, two dielectric resonator antennas, and a patch antenna.**

***Index Terms*— Dielectric antennas, partial element equivalent circuit method (PEEC), passivity.**

I. Introduction

MODERN electronic packaging for high-speed and high-frequency systems involves high-density conductor routings and finite-dimension unstructured homogenous dielectrics. The problem may involve complicated electromagnetic (EM) phenomena, such as electric and magnetic coupling, radiation effect, and conductor and dielectric losses, which aggravate the difficulties of the signal integrity (SI) and EM compatibility (EMC) analysis. Accurately modeling a packaging and EMC problem requires a full-wave description of these EM phenomena [1].

Among various EM modeling methods, including method of moments [2], finite-element method [3], and finite-difference time-domain method [4], the partial element equivalent circuit (PEEC) model [5]–[7] is the only method that can convert an EM problem into a mesh-based circuit problem, which can be solved efficiently by a SPICE-like solver. The PEEC model can serve as a good starting point to derive a concise physically meaningful circuit that incorporates all the physically sensible inductive and capacitive coupling as well as the radiation effect. For a large-scale PEEC model, a recently developed model order reduction can be applied to find a concise passive physically meaningful micromodeling circuit [8], of which the order of a PEEC model can be reduced by one order of magnitude and the computation time for system responses can be reduced by about three orders of magnitude.

The radiation effect in PEEC modeling for multiconductor problems or microstrip structure problems has been thoroughly studied [9]–[11]. In [9] and [10], the frequency-dependent radiation resistance of each current cell on conductors is found to be the imaginary part of the generalized inductance, while static capacitance, which is defined in a conservative electric field, is preserved. The radiation resistance of the free-space PEEC model is proved to be equal to the well-known radiation resistance of a short electric dipole with a uniform current distribution. It has been proved that the generalized inductance concept is consistent with the Poynting theorem in the frequency domain [12]. A recent study on a passive micromodeling circuit reveals that the PEEC model with the static capacitance can be enforced to be passive for the time-domain simulation [13] without altering the circuit configuration.

To correctly model an EM problem in the time domain, the retarded PEEC model [6], [7] interprets the phase difference between the source and observation points by a time delay, which is a proper approximation for far-field coupling. However, the time delay of the self-term, which is essential for modeling radiation phenomenon in the frequency domain, is approximated to be zero. The retarded Taylor expansion PEEC model [14] overcomes this problem by introducing frequency-dependent circuit elements along with the retardation. However, in the retarded Taylor expansion PEEC model, the equivalent resistances on the charge cell are negative, which is nonpassive in circuit theory. A time-domain analysis of a full-wave PEEC model is introduced in [15], by which the time-domain response of a frequency-dependent PEEC model can be expressed as a summation of time-domain responses of several static subcircuits that are obtained by sampling the full-wave PEEC model at the respective frequency points.

In this article, a generalized full-wave 3-D PEEC model for irregularly shaped composite conductor–dielectric EM problems is proposed. The problem is formulated by the mixed potential integral equation (MPIE) on closed surface boundaries, which are discretized by triangular meshes and Rao–Wilton–Glisson (RWG) basis functions [16]. This article

Manuscript received December 27, 2018; revised May 24, 2019 and August 28, 2019; accepted September 15, 2019. Date of publication November 7, 2019; date of current version January 13, 2020. This work was supported in part by the Research Grants Council of the Hong Kong Special Administrative Region, China, under Grant 14205217. *(Corresponding author: Ke-Li Wu.)*

The authors are with the Department of Electronic Engineering, The Chinese University of Hong Kong, Hong Kong (e-mail: jiangy@ee.cuhk.edu.hk; klwu@cuhk.edu.hk).

Color versions of one or more of the figures in this article are available online at http://ieeexplore.ieee.org.

Digital Object Identifier 10.1109/TMTT.2019.2947912

formulates an EM problem by real-valued frequency variant electric and magnetic inductors, radiation resistors, and static capacitance for the first time. Unlike the traditional complex LC S-PEEC model for the EM problems involving conductors and dielectrics of finite size [7], the proposed generalized PEEC model accounts for the radiation effects of both conductors and dielectrics by introducing frequency-dependent radiation resistances. The PEEC model consists of frequency-invariant real capacitors for charge cells and complex self- and mutual inductors for current cells, each of which alternatively represents a radiation resistance in series with a real inductance. Similar to [13], the passivity of the resulting circuit model in the frequency domain is verified numerically by normalized passivity violation (NPV) factors. The passivity of the proposed PEEC model is verified by four practical problems: a multilayer embedded RF filter, a wide-band dielectric resonator antenna (DRA), a slot-coupled DRA, and a patch antenna with finite substrate. The results are compared with those obtained by the commercial software with very good agreement. It is worth mentioning that it is for the first time to demonstrate that a PEEC model can accurately model the radiation of dielectrics of finite size.

This article is organized as follows. In Section II, the integral equations based on the surface equivalence principle are briefly outlined. Section III discusses the advantage of the triangular meshing scheme for the PEEC model. The discretized integrations using the RWG basis are briefly discussed in Section IV. In Section V, the generalized PEEC model is presented. It is analytically proven in Section VI that the self-radiation resistance is guaranteed to be positive. Section VII introduces the passivity-checking method of the proposed PEEC circuit model in the frequency domain. Four practical examples are given in Section VIII, followed by the conclusion.

II. Equivalent Principle and Integral Equations

The surface equivalence principle is widely used for modeling EM problems including finite homogeneous dielectrics in the method of moments (MoM) and traditional S-PEEC model, which is also used in the proposed generalized PEEC model. For completeness and clearness, the surface equivalence principle is briefly introduced in this section.

The equivalence principle is illustrated in Fig. 1 by a typical EM problem that contains two dielectrics $\{D_1, D_2\}$ with permittivity $\{\varepsilon_1, \varepsilon_2\}$ and three pieces of conductors $\{C_0, C_1, C_2\}$ that are located in the background environment, D_1 and D_2, respectively. The permittivity of the background environment is assumed to be ε_0. As shown in Fig. 1(a), the dielectrics and conductors are bounded by surfaces $\{s_1^D, s_2^D\}$ and $\{s_0^C, s_1^C, s_2^C\}$. If the dielectrics touch each other, there is an infinitely small gap δd between the contact dielectrics. The dielectric surfaces divide the problem domain into three regions. A hypothetic surface s_0^D for the *0*th region includes s_1^D, s_2^D and the surface at infinite. According to the surface equivalence principle, the original EM problem is equivalent to three subproblems, as shown in Figs. 1(b), (c), and (d). In each of the subproblem, equivalent electric and magnetic currents will

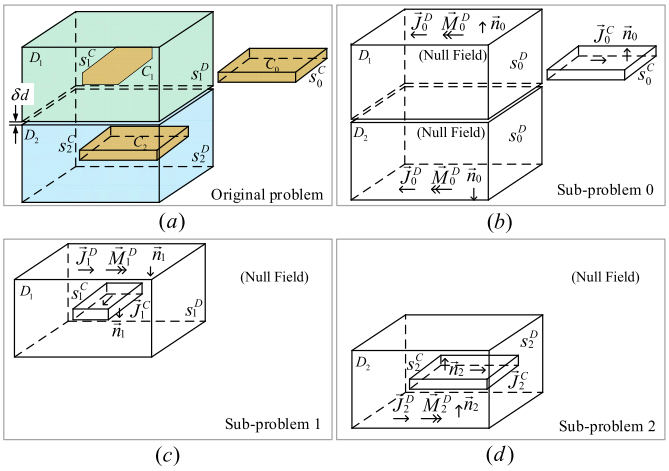

Fig. 1. Problem contains multiple conductors and finite-sized dielectrics and its equivalence subproblems. (a) Original problem. (b) Subproblem 0 with true fields inside s_0^D. (c) Subproblem 1 with true fields inside s_1^D. (d) Subproblem 2 with true fields inside s_2^D.

produce the true fields inside the corresponding region and a null field elsewhere. The equivalent electric current density $\vec{J}_i$, magnetic current density $\vec{M}_i$, electric charge density ρ_i, and magnetic charge density σ_i are defined by

$$\vec{J}_i(r) = \vec{n}_i \times \vec{H}(r), \quad \vec{M}_i(r) = \vec{E}(r) \times \vec{n}_i \tag{1}$$

$$\rho_i(r) = -\nabla \cdot \vec{J}_i(r)/j\omega, \quad \sigma_i(r) = -\nabla \cdot \vec{M}_i(r)/j\omega \tag{2}$$

where $\vec{n}_i$ is the unit normal vector of $s_i^{C,D}$ pointing to the true field region and $r \in s_i^{C,D} (i = 0, 1, 2)$. As the tangential fields are continuous across the boundary of dielectrics, the equivalent surface sources on dielectric surfaces $\vec{J}^D$ and $\vec{M}^D$ hold the properties on s_i^D that

$$\vec{J}_0^D(r) = -\vec{J}_i^D(r), \quad \vec{M}_0^D(r) = -\vec{M}_i^D(r) \tag{3}$$

in which $i = 1, 2$. By applying the boundary condition that the tangential electric and magnetic fields on two sides of the dielectric surfaces are continuous and the tangential electric field on conductor surfaces is zero, the following equations can be acquired:

$$\vec{n}_i \times [\vec{E}_0(r^+) - \vec{E}_i(r^-)]|_{s_i^D} = 0,$$

$$\vec{n}_i \times [\vec{H}_0(r^+) - \vec{H}_i(r^-)]|_{s_i^D} = 0 \tag{4}$$

$$\vec{n}_i \times \vec{E}_i(r^+)|_{s_i^C} = -\vec{n}_i \times \vec{E}_i^{\text{inc}}(r^+)|_{s_i^C} \tag{5}$$

where r^+ and r^- are the position of observation points, which approach to the point r on the surface $s_i^{C,D}$ from outside and inside, respectively. $\vec{E}_i$ and $\vec{H}_i$ follow the well-known electric field integral equation (EFIE) and magnetic field integral equation (MFIE) in a homogeneous space with permittivity ε_i

$$\vec{E}_i(r) = -j\omega\vec{A}_i(r) - \nabla\phi_i(r) - \nabla \times \frac{1}{\varepsilon_i}\vec{F}_i(r) \tag{6}$$

$$\vec{H}_i(r) = -j\omega\vec{F}_i(r) - \nabla\varphi_i(r) + \nabla \times \frac{1}{\mu_0}\vec{A}_i(r) \tag{7}$$

in which the potential functions for the ith subproblem are given by

$$\vec{A}_i(r) = \mu_0 \int G_i(r,r')\vec{J}_i(r')ds \tag{8}$$

$$\vec{F}_i(r) = \varepsilon_i \int G_i(r,r')\vec{M}_i(r')ds \tag{9}$$

$$\phi_i(r) = \frac{1}{\varepsilon_i} \int G_i(r,r')\rho_i(r')ds \tag{10}$$

$$\varphi_i(r) = \frac{1}{\mu_0} \int G_i(r,r')\sigma_i(r')ds \tag{11}$$

where $G_i(r,r')$ is the full-wave Green's function in a homogenous space of permittivity ε_i

$$G_i(r,r') = \frac{\exp(-jk_iR)}{4\pi R} \tag{12}$$

in which $R = |r - r'|$ and wavenumber $k_i = \omega(\mu_0\varepsilon_i)^{1/2}$.

By substituting the electric and magnetic fields of (6) and (7) into (4) and (5), the MPIEs can be obtained as follows [7]:

On the Dielectric Surface s_i^D:

$$\vec{n}_i \times \left\{ -j\omega\left[\vec{A}_0(r^+) - \vec{A}_i(r^-)\right] - \nabla\left[\phi_0(r^+) - \phi_i(r^-)\right] - \nabla \times \left[\frac{1}{\varepsilon_0}\vec{F}_0(r^+) - \frac{1}{\varepsilon_i}\vec{F}_i(r^-)\right]\right\} = 0 \tag{13}$$

$$\vec{n}_i \times \left\{ -j\omega\left[\vec{F}_0(r^+) - \vec{F}_i(r^-)\right] - \nabla\left[\varphi_0(r^+) - \varphi_i(r^-)\right] + \nabla \times \left[\frac{1}{\mu_0}\vec{A}_0(r^+) - \frac{1}{\mu_0}\vec{A}_i(r^-)\right]\right\} = 0. \tag{14}$$

On the Conductor Surface s_i^C:

$$\vec{n}_i \times \left\{ -j\omega\vec{A}_i(r^+) - \nabla\phi_i(r^+) - \nabla \times \frac{1}{\varepsilon_0}\vec{F}_0(r^+)\right\} = -\vec{n}_i \times \vec{E}_i^{\text{inc}}(r^+). \tag{15}$$

III. Discretization With RWG Basis Function

The RWG basis function [16] is widely used in the MoM for discretizing surface currents with triangular meshes. In the proposed generalized PEEC method, triangular meshes and the RWG basis function are adopted. Each adjacent triangular mesh pair forms one RWG basis. The basis function of the kth mesh pair, referring to Fig. 2(a) and (b), is defined by

$$\vec{b}_k(r) = \begin{cases} \pm\dfrac{L_k}{2A_k^+}\vec{v}^{\pm}, & r \in S_{k^\pm} \\ 0, & \text{otherwise} \end{cases} \tag{16}$$

where $\vec{v}^{\pm}$ is the vector from the vertex opposite to the common edge pointing to the source point, and L_k is the length of the interior edge between a pair of meshes T_k^+ and T_k^-, whose areas are A_k^+ and A_k^-, respectively.

Assume the surfaces are divided into $N = N_C + N_D$ triangular meshes forming $M = M_C + M_D$ current cells, in which the subscripts stand for conductor (C) or dielectric (D). The discretized current density functions can be written as

$$\vec{J}(r) = \sum_{k=1}^{M} \frac{1}{L_k}\vec{b}_k(r)I_k^E, \quad \vec{M}(r) = \sum_{k=1}^{M_D} \frac{Z_0}{L_k}\vec{b}_k(r)I_k^H \tag{17}$$

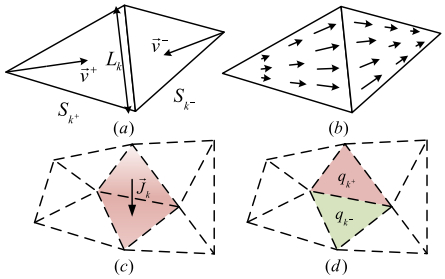

Fig. 2. kth mesh element for RWG basis function. (a) Geometrical parameter. (b) Vector basis function. (c) kth current cell for inductance. (d) Two charge cells k^+ and k^- for capacitance.

in which $I^{E,H}$ are the discretized electric/magnetic surface currents. As the unit of magnetic current density $\vec{M}$ is in V/m, a constant $Z_0 = (\mu_0/\varepsilon_0)^{1/2}$ should be multiplied on the discretized magnetic current to enforce the unit of the equivalent magnetic current to be in A. The basis for charge densities can also be obtained directly by substituting the discretized current density functions (17) into the current continuity function (2). Taking the electric charge density on the lth mesh as an example

$$\rho(r) = -\frac{1}{j\omega}\nabla \cdot \sum_{k=1}^{M} \frac{1}{L_k}\vec{b}_k(r)I_k^E = -\frac{1}{j\omega A_l}\sum_{i=1}^{3} \pm I_{l_i}^E \tag{18}$$

where $\pm I_{l_i}^E$ is the electric surface current flowing out of (+) or into (−) the lth mesh. As the equivalent currents and A_l are constant, the charge density is naturally a constant over each triangular mesh. The charge density distributions can be represented by

$$\rho(r) = \frac{1}{j\omega}\sum_{l=1}^{N} f_l(r)I_l^{E_{\text{Dis}}}, \quad \sigma(r) = \frac{1}{j\omega}\sum_{l=1}^{N_D} Z_0 f_l(r)I_l^{H_{\text{Dis}}} \tag{19}$$

in which $I^{E,H_{\text{Dis}}}$ are the electric/magnetic displacement currents and

$$f_l(r) = \begin{cases} \dfrac{1}{A_l}, & r \in S_l \\ 0, & \text{otherwise.} \end{cases} \tag{20}$$

In the proposed PEEC model, every adjacent mesh pair forms one *current* cell and every mesh itself is a *charge* cell as shown in Fig. 2(c) and (d). Referring to (18) and (19), the following relation can be found:

$$I_l^{E,H_{\text{Dis}}} = \sum_{i=1}^{3} \pm I_{l_i}^{E,H} \tag{21}$$

which indicates that the total equivalent surface currents flowing into a charge cell equal the displacement current $I^{E,H_{Dis}}$ flowing from the charge cell into the ground at infinite.

Compared with the quadrilateral meshing scheme, the triangular meshing scheme can fit an irregularly shaped surface with fewer unknowns. In addition, the RWG basis is a first-order basis function, with which the gradient of the equivalent currents is a constant charge distribution on every charge cell.

IV. Discrete Integral Equations With RWG Basis

After discretizing and Garlerkin matching of (13)–(15), a set of discretized integral equations can be acquired. The EFIE (13) and MFIE (14) introduce two sets of equations on dielectric surfaces and one set of equations on conductor surfaces. The discretized integral equations can be expressed in a matrix form as

$$\begin{bmatrix} j\omega M^E & Z^E \\ Z^H & j\omega M^H \end{bmatrix} \begin{bmatrix} I^E \\ I^H \end{bmatrix} = \frac{1}{j\omega}[A]^T \begin{bmatrix} P^E & 0 \\ 0 & P^H \end{bmatrix} \begin{bmatrix} I^{E_{\mathrm{Dis}}} \\ I^{H_{\mathrm{Dis}}} \end{bmatrix} + \begin{bmatrix} V_{\mathrm{inc}} \\ 0 \end{bmatrix} \quad (22)$$

in which $[A]^T$ is the transpose of the connectivity matrix $[A]$, in which entry A_{ij} is 1 or -1 if the current on the jth current cell flows out of or into the ith charge cell, otherwise is 0. Therefore, (21) can be written in a matrix form as

$$\begin{bmatrix} I^{E_{\mathrm{Dis}}} \\ I^{H_{\mathrm{Dis}}} \end{bmatrix} = -[A] \begin{bmatrix} I^E \\ I^H \end{bmatrix}. \quad (23)$$

In (22) and (23), $I^{E,H}$, $I^{E,H_{Dis}}$, and V_{inc} are the vectors of electric/magnetic surface currents, displacement currents, and excitation sources, respectively. The entries of submatrices $M^{E,H}$, $Z^{E,H}$, and $P^{E,H}$ in (22) are defined by

$$M^E_{mk} = \frac{\mu_0}{L_m L_k} \int_{S_m} \int_{S_k} (H_0 G_0 - H_i G_i) \vec{b}_m \cdot \vec{b}'_k ds' ds \quad (24)$$

$$M^H_{mk} = \frac{\mu_0}{L_m L_k} \int_{S_m} \int_{S_k} (H_0 G_0 - \varepsilon_{r_i} H_i G_i) \vec{b}_m \cdot \vec{b}'_k ds' ds \quad (25)$$

$$Z^{EH}_{mk} = \frac{Z_0}{L_m L_k} \int_{S_m} \int_{S_k} (H_0 \nabla G_0 - H_i \nabla G_i) \cdot (\vec{b}_m \times \vec{b}'_k) ds' ds \quad (26)$$

$$Z^{HE}_{mk} = -\frac{Z_0}{L_m L_k} \int_{S_m} \int_{S_k} (H_0 \nabla G_0 - H_i \nabla G_i) \cdot (\vec{b}_m \times \vec{b}'_k) ds' ds \quad (27)$$

$$P^E_{ml} = \frac{1}{\varepsilon_0 A_m A_l} \int_{S_m} \int_{S_l} \left(H_0 G_0 - \frac{H_i G_i}{\varepsilon_{r_i}} \right) ds' ds \quad (28)$$

$$P^H_{ml} = \frac{1}{\varepsilon_0 A_m A_l} \int_{S_m} \int_{S_l} (H_0 G_0 - H_i G_i) ds' ds. \quad (29)$$

The weighting function H_i in (24)–(29) describes the coupling relationship between the testing cells and the source cells.

For $i = 0$

$$H_0(r, r') = \begin{cases} 1, & r \in s^0_{C,D} \text{ and } r' \in s^0_{C,D} \\ 0, & \text{otherwise.} \end{cases} \quad (30)$$

For $i = 1, 2$

$$H_i(r, r') = \begin{cases} -1, & r \in s^i_{C,D} \text{ and } r' \in s^i_{C,D} \\ 0, & \text{otherwise} \end{cases} \quad (31)$$

where the weighting function $H_i(r, r')$ is nonzero if and only if the observation point r and the source point r' are on the surfaces of the same subproblem. In defining the function $H_i(r, r')$, relation (3) is used.

The first term on the right-hand side (RHS) of (22) is defined as the potential differences between two neighboring nodes.

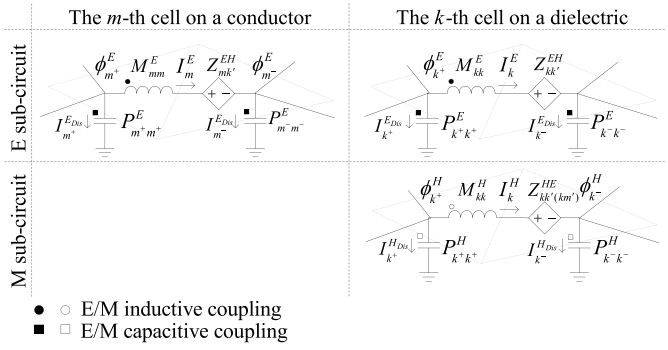

Fig. 3. Circuit representation of discrete integral equations: the mth current cell on a conductor surface and the kth current cell on a dielectric surface.

The potentials at nodes are defined by

$$\begin{bmatrix} \phi^E \\ \phi^H \end{bmatrix} = \frac{1}{j\omega} \begin{bmatrix} P^E & 0 \\ 0 & P^H \end{bmatrix} \begin{bmatrix} I^{E_{\mathrm{Dis}}} \\ I^{H_{\mathrm{Dis}}} \end{bmatrix}. \quad (32)$$

The discretized integral equations (22) and (23) can be interpreted as KVL and KCL equations. The EFIE (13) and MFIE (14) introduce two subcircuits on dielectric surfaces, namely, electric (E) subcircuit and magnetic (M) subcircuit. As shown in Fig. 3, the E subcircuit describes both conductors and dielectrics, whereas the M subcircuit is used only for the magnetic currents on the surfaces of dielectrics, where the circle dot and square dot symbols represent the inductive and capacitive couplings, respectively. Each self- or mutual-inductance $M^{E,H}$ is in series with multiple current-controlled voltage sources (CCVS) $Z^{EH,HE}$. The CCVSs in the E/M subcircuits are controlled by the equivalent magnetic/electric currents in the other subcircuits.

In the traditional complex LC PEEC model, a *complex* capacitance $P^{E,H}$ connects a charge cell and the ground at infinite. The complex self- or mutual-capacitance is interpreted as a real-valued capacitance in series with a resistance or resistive coupling [11]. It is further proved analytically that the self-resistance must be negative. Obviously, the negative self-resistances violate the passivity property of the PEEC model. The complex LC PEEC model for dielectrics of finite size also exhibits the nonpassive attribute.

V. Generalized PEEC Model

In [9] and [10], the generalized PEEC models for problems of homogeneous environment and layered dielectrics are proposed. The generalized PEEC model with frequency-independent capacitances for homogeneous space problems has been proven to be stable for the time-domain simulation [13]. In this work, the concept of static capacitance is applied in the proposed generalized PEEC model for modeling EM problems including dielectrics of finite sizes.

The potential coefficients $P^{E,M}$ in (28) and (29) can be decomposed into a frequency-independent static term and a frequency-dependent term. Taking the electric potential coefficient between the mth and the lth charge cells as an example

$$P^E_{ml} = \bar{P}^E_{ml} + \tilde{P}^E_{ml} \quad (33)$$

and

$$\bar{P}^E_{ml} = \frac{1}{\varepsilon_0 A_m A_l}\int_{S_m}\int_{S_l} \bar{G}H_0 - \frac{\bar{G}H_i}{\varepsilon_{r_i}} ds' ds \tag{34}$$

$$\tilde{P}^E_{ml} = \frac{1}{\varepsilon_0 A_m A_l}\int_{S_m}\int_{S_l} (G_0 - \bar{G})H_0 - \frac{(G_i - \bar{G})}{\varepsilon_{r_i}} H_i ds' ds \tag{35}$$

where $\bar{P}^E_{ml}$ is frequency-independent and $\tilde{P}^E_{ml}$ is frequency-dependent. Function $\bar{G} = 1/4\pi|r - r'|$ is the static Green's function. The potential coefficient matrix on the RHS of (22) can be written as

$$\begin{bmatrix} P^E & 0 \\ 0 & P^H \end{bmatrix} = \begin{bmatrix} \bar{P}^E & 0 \\ 0 & \bar{P}^H \end{bmatrix} + \begin{bmatrix} \tilde{P}^E & 0 \\ 0 & \tilde{P}^H \end{bmatrix}. \tag{36}$$

Considering (23) and (36), (22) can be rewritten as

$$\begin{bmatrix} j\omega M^E & Z^E \\ Z^H & j\omega M^H \end{bmatrix}\begin{bmatrix} I^E \\ I^H \end{bmatrix} + \frac{1}{j\omega}[A]^T \begin{bmatrix} \tilde{P}^E & 0 \\ 0 & \tilde{P}^H \end{bmatrix}[A]\begin{bmatrix} I^E \\ I^H \end{bmatrix} = [A]^T \begin{bmatrix} \bar{\phi}^E \\ \bar{\phi}^H \end{bmatrix} + \begin{bmatrix} V_{\text{inc}} \\ 0 \end{bmatrix} \tag{37}$$

where the updated node potentials $\bar{\phi}^{E,H}$ are consistent with the potentials defined in a conservative field

$$\begin{bmatrix} \bar{\phi}^E \\ \bar{\phi}^H \end{bmatrix} = \frac{1}{j\omega}\begin{bmatrix} \bar{P}^E & 0 \\ 0 & \bar{P}^H \end{bmatrix}\begin{bmatrix} I^{E_{\text{Dis}}} \\ I^{H_{\text{Dis}}} \end{bmatrix}. \tag{38}$$

As there is no direct connection between the E and M subcircuits, the connective matrix $[A]$ can be expressed as

$$[A] = \begin{bmatrix} A_E & 0 \\ 0 & A_H \end{bmatrix} \tag{39}$$

in which $A_{E,H}$ is the connective matrix for the E and M subcircuits. By replacing $[A]$ and $[A]^T$ in (37) by (39), the second term on the left-hand side (LHS) of (37) can be represented by

$$\frac{1}{j\omega}[A]^T \begin{bmatrix} \tilde{P}^E & 0 \\ 0 & \tilde{P}^H \end{bmatrix}[A]\begin{bmatrix} I^E \\ I^H \end{bmatrix} = \frac{1}{j\omega}\begin{bmatrix} A_E \tilde{P}^E A_E^T & 0 \\ 0 & A_H \tilde{P}^H A_H^T \end{bmatrix}\begin{bmatrix} I^E \\ I^H \end{bmatrix}. \tag{40}$$

The entries of $[A_{E,H}\tilde{P}^{E,H}A^T_{E,H}]$ for the E and M subcircuits on the RHS of (40), which is denoted as $p^{E,H}_{mk}$, are evaluated as

$$p^{E,H}_{mk} = \tilde{P}^{E,H}_{m^+k^+} + \tilde{P}^{E,H}_{m^-k^-} - \tilde{P}^{E,H}_{m^-k^+} - \tilde{P}^{E,H}_{m^+k^-} \tag{41}$$

in which the subscripts $m^\pm$ and $k^\pm$ of the potential coefficient are the indexes of the charge cells from which the mth and the kth currents flow out (+) or in (−). Replacing the second term on the LHS of (37) by (40) yields

$$\begin{bmatrix} j\omega\bar{M}^E & Z^{EH} \\ Z^{HE} & j\omega\bar{M}^H \end{bmatrix}\begin{bmatrix} I^E \\ I^H \end{bmatrix} = [A]^T \begin{bmatrix} \bar{\phi}^E \\ \bar{\phi}^H \end{bmatrix} + \begin{bmatrix} V_{\text{inc}} \\ 0 \end{bmatrix} \tag{42}$$

where $j\omega\bar{M}^{E,H}$ is impedance matrices that absorb the frequency-dependent terms of potential coefficient $\tilde{P}^{E,H}$ by

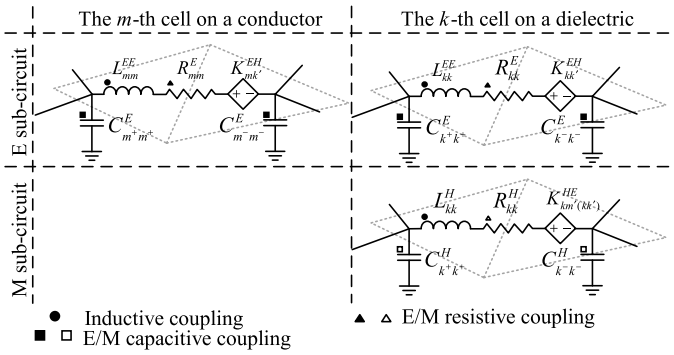

Fig. 4. Generalized PEEC model: the mth current cell on a conductor surface and the kth current cell on a dielectric surface.

the inductance matrix $M^{E,H}$. The entries of $\bar{M}^{E,H}$ are given by

$$\bar{M}^{E,H}_{mk} = M^{E,H}_{mk} - \frac{\tilde{P}^{E,H}_{m^+k^+} + \tilde{P}^{E,H}_{m^-k^-} - \tilde{P}^{E,H}_{m^-k^+} - \tilde{P}^{E,H}_{m^+k^-}}{\omega^2}. \tag{43}$$

The complex coupling on the LHS of (42) can be decomposed into two frequency-dependent parts: real and imaginary. Each part is interpreted as a circuit element: the inductive coupling $L^{EE,HH}$ along with the resistive coupling $R^{E,H}$, or

$$L^{EE,HH}_{mk} = \text{Re}\big(\bar{M}^{E,H}_{mk}\big) \quad \text{and} \quad R^{E,H}_{mk} = -\omega\text{Im}\big(\bar{M}^{E,H}_{mk}\big). \tag{44}$$

It can be noticed that $j\omega\bar{M}^{E,H} = j\omega L^{EE,HH} + R^{E,H}$. Similarly, $Z^{EH,HE}$ are regarded as CCVS of $K^{EH,HE}$ along with the inductive coupling $M^{EH,HE}$, which are defined as

$$K^{EH,HE}_{mk} = \text{Re}\big(Z^{EH,HE}_{mk}\big) \quad \text{and} \quad L^{EH,HE}_{mk} = \frac{1}{\omega}\text{Im}\big(Z^{EH,HE}_{mk}\big). \tag{45}$$

Meanwhile, $\bar{P}^{E,H}$ in (38) defines the potential coefficients. According to the definition, $\bar{P}^{E,H}$ can be referred to as the potential coefficients for the capacitance $C^{E,H}$, which connects charge cells and the ground, that is,

$$\begin{bmatrix} C^E & 0 \\ 0 & C^H \end{bmatrix} = \begin{bmatrix} \bar{P}^E & 0 \\ 0 & \bar{P}^H \end{bmatrix}^{-1} \tag{46}$$

where $C^{E,H}$ is the inverse matrix of the potential coefficient matrix $\bar{P}^{E,H}$. Referring to (23), (38), and (46), one can find

$$j\omega\begin{bmatrix} C^E & 0 \\ 0 & C^H \end{bmatrix}\begin{bmatrix} \bar{\phi}^E \\ \bar{\phi}^H \end{bmatrix} = -[A]\begin{bmatrix} I^E \\ I^H \end{bmatrix}. \tag{47}$$

Finally, the generalized PEEC model with real-valued circuit elements for problems, including dielectrics of finite size, is acquired. The equivalent circuits of the mth current cell on a conductor and the kth current cell on a dielectric along with the couplings are illustrated in Fig. 4. On current meshes, each inductor is in series with a resistor along with mutual coupling with other inductors or resistors. Mutual coupling exists among the static capacitors and the ground at infinite. In addition, (42), (44), (45), and (47) can be combined into

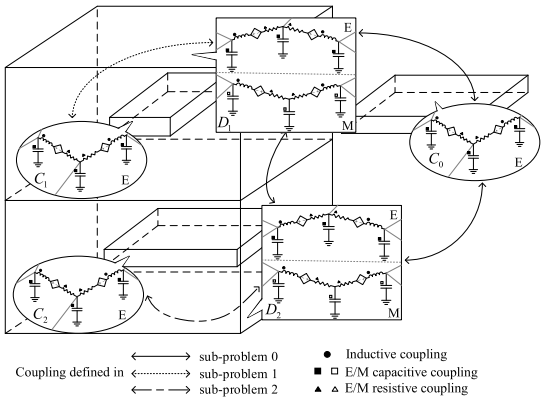

Fig. 5. Subcircuits of the generalized PEEC model on conductor and dielectric surfaces, where the coupling between subcircuits is presented by two-head arrows.

a modified nodal analysis (MNA) matrix [17] as

$$\begin{bmatrix} j\omega L^{EE}+R^E & j\omega L^{EH}+K^E & -A^T & \\ j\omega L^{HE}+K^H & j\omega L^{HH}+R^H & & \\ A & & j\omega C^E & 0 \\ & & 0 & j\omega C^H \end{bmatrix} \times \begin{bmatrix} I^E \\ I^H \\ \bar{\phi}^E \\ \bar{\phi}^H \end{bmatrix} = \begin{bmatrix} V_{\text{inc}} \\ 0 \\ 0 \\ 0 \end{bmatrix}. \quad (48)$$

By now, the whole picture of the generalized PEEC model can be shown in Fig. 5. The resulting PEEC model is described by five subcircuits. The three subcircuits on conductor surfaces $\{s_0^C, s_1^C, s_2^C\}$ and two subcircuits on dielectric surfaces $\{s_1^D, s_2^D\}$ are depicted in the elliptic- and rectangular-shaped blocks, respectively. In each subcircuit, coupling among circuit elements is self-contained. Coupling among the five subcircuits is described by the three subproblems defined in Fig. 1. The properties of the generalized PEEC model are summarized as follows.

1) The electric and magnetic currents on dielectric surfaces will coexist in two sets of separate subcircuits, electric (E) subcircuit, and magnetic (M) subcircuit. On conductor surfaces, only an electric subcircuit exists.
2) Inductive coupling exists among not only the same type of subcircuits but also among E and M subcircuits; resistive and capacitive coupling appear only among E or M subcircuits.
3) The CCVS on E subcircuits is controlled by the current on M subcircuits, and vice versa.
4) The coupling among circuit elements on different surfaces exists only if the surfaces belong to the same subproblem.
5) All the partial circuit elements are frequency-dependent except the capacitances and their mutual coupling.
6) All the couplings are symmetric except the CCVS of $K^{EH,HE}$ and the inductive coupling $L^{EH,HE}$.

By comparing (26) and (27), it can be found that the CCVS and inductive coupling, which reflect the coupling between the E subcircuits and the M subcircuits, are opposite to each other, that is, $[K^{EH}] = -[K^{HE}]^T$ and $[L^{EH}] = -[L^{HE}]^T$ in a matrix form. The asymmetric property of the inductive coupling is in consistent with the definition of the radiative power in the circuit domain as discussed in Section VI.

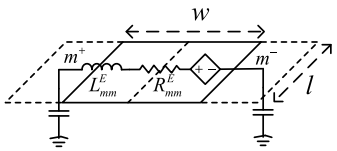

Fig. 6. Circuit on mth rectangular mesh pair and meshes' physical dimensions.

VI. Radiation Resistances

For a lossless problem, the total radiating power P_{rad} equals the power consumed in the generalized PEEC model, which can be expressed as

$$\begin{aligned} P_{\text{rad}} = \text{Re}\Bigg\{ & \begin{bmatrix} I^{E^{*T}} & I^{H^{*T}} \end{bmatrix} \\ & \times \begin{bmatrix} j\omega L^{EE}+R^E & j\omega L^{EH}+K^E \\ j\omega L^{HE}+K^H & j\omega L^{HH}+R^H \end{bmatrix} \begin{bmatrix} I^E \\ I^H \end{bmatrix} \Bigg\} \\ & + \text{Re}\Bigg\{ \begin{bmatrix} \bar{\phi}^{E^{*T}} & \bar{\phi}^{H^{*T}} \end{bmatrix} \begin{bmatrix} j\omega C^E & 0 \\ 0 & j\omega C^H \end{bmatrix} \begin{bmatrix} \bar{\phi}^E \\ \bar{\phi}^H \end{bmatrix} \Bigg\} \end{aligned} \quad (49)$$

in which $[X^*]^T$ is the transpose conjugate of $[X]$. $[X]$ is a place holder of current vectors $[I^{E,H}]$ and potential vectors $[\phi^{E,H}]$. Be reminded that: 1) all the circuit elements are real; 2) submatrices $[j\omega L^{EE,HH}+R^{E,H}]$ are symmetric; and 3) the couplings between E and M subcircuits are opposite, that is, $[j\omega L^{EH}+K^E] = -[j\omega L^{HE}+K^H]^T$, the RHS of (49) can be summarized as

$$\begin{aligned} P_{\text{rad}} = & \sum_{i=1}^{M}\sum_{j=1}^{M} R_{ij}^E \text{Re}\big(I_i^E I_j^E\big) + \sum_{i=1}^{M_D}\sum_{j=1}^{M_D} R_{ij}^H \text{Re}\big(I_i^H I_j^H\big) \\ & + \omega \sum_{i=1}^{M}\sum_{j=1}^{M_D} L_{ij}^{EH} \text{Im}\big(I_i^E I_j^H\big) \\ & + \omega \sum_{i=1}^{M_D}\sum_{j=1}^{M} L_{ij}^{HE} \text{Im}\big(I_i^E I_j^H\big) \end{aligned} \quad (50)$$

which indicates that the radiation is contributed by the resistive couplings within E and M subcircuits and the inductive couplings between E and M subcircuits in the generalized PEEC model.

To reveal the physical meaning of the self-radiation resistance analytically, a pulse basis is used in a current mesh (solid line) and charge meshes (dashed line) shown in Fig. 6 in the following derivation. In (43), five terms on the RHS contribute to the electric radiation resistance R_{mm}^E when $k = m$. For the self-coupling terms $\tilde{P}_{m^\pm m^\pm}^E$ and M_{mm}^E, as the distance R between the source and the observation points approaches to 0, the first-order Taylor expansion of the exponential factor in Green's function can be made by

$$e^{-jkR} \approx 1 - jkR. \quad (51)$$

Consequently, M^E_{mm} can be represented by

$$M^E_{mm} = \frac{\mu_0}{4\pi w^2}\int_{S_m}\int_{S_m}\frac{e^{-jk_0R}}{R}+\frac{e^{-jk_rR}}{R}ds'ds \approx \frac{\mu_0}{4\pi w^2}\int_{S_m}\int_{S_m}\frac{2}{R}ds'ds - \frac{j\mu_0 l^2(k_0+k_r)}{4\pi} \quad (52)$$

where l and w are the length and width of a current mesh, respectively. Similarly, $\tilde{P}^E_{m^\pm m^\pm}$ can be expressed as

$$\tilde{P}^E_{m^\pm m^\pm} = \frac{1}{4\pi\varepsilon_0 A_{m^\pm}A_{m^\pm}}\int_{S_{m^\pm}}\int_{S_{m^\pm}}\frac{e^{-jk_0R}-1}{R} + \frac{e^{-jk_rR}-1}{\varepsilon_r R}ds'ds \approx -\frac{j}{4\pi\varepsilon_0}\left(k_0+\frac{k_r}{\varepsilon_r}\right). \quad (53)$$

When the source and the observation points are not on the same mesh for the intercoupling terms $\tilde{P}^E_{m^\pm m^\mp}$, the fourth-order Taylor series approximation gives

$$e^{-jkR} \approx 1 - jkR - \frac{(kR)^2}{2!} + \frac{j(kR)^3}{3!}. \quad (54)$$

By setting $R \approx l$, the intercoupling terms can be expressed as

$$\tilde{P}^E_{m^\pm m^\mp} = \frac{1}{4\pi\varepsilon_0 A_{m^\pm}A_{m^\mp}}\int_{S_{m^\pm}}\int_{S_{m^\mp}}\frac{e^{-jk_0R}-1}{R} + \frac{e^{-jk_rR}-1}{\varepsilon_r R}ds'ds \approx -\frac{j}{4\pi\varepsilon_0}\left(k_0+\frac{k_r}{\varepsilon_r}\right) - \frac{\mu_0\omega^2 l}{4\pi} + \frac{j\mu_0\omega^2 l^2}{24\pi}(k_0+k_r). \quad (55)$$

Having had the above approximations, the generalized electric self-inductance can be expressed as

$$L^{EE}_{mm} = \mathrm{Re}\big(\bar{M}^E_{mm}\big) \approx \frac{\mu_0}{2\pi w^2}\int_{S_m}\int_{S_m}\frac{1}{R}ds'ds - \frac{\mu_0 l}{2\pi} \quad (56)$$

and the radiation resistance can be easily found as

$$R^E_{mm} = -\omega\mathrm{Im}\big(\bar{M}^E_{mm}\big) = \frac{\omega\mu_0 l^2}{6\pi}(k_0+k_r) = 80\pi^2[(l/\lambda_0)^2 + (l/\lambda_r)^2/\sqrt{\varepsilon_r}] \quad (57)$$

where $\lambda_{0,r} = 2\pi/k_{0,r}$, which is the wavelength in the free-space with the relative permittivity of 1 or ε_r. In deriving (57), the approximation of $\mu_0{\varepsilon_0}^{1/2} \approx 120\pi$ is used. By the same token, the generalized inductance for a magnetic current cell can be found as

$$L^{HH}_{mm} \approx \frac{\mu_0}{4\pi w^2}\int_{S_m}\int_{S_m}\frac{1+\varepsilon_r}{R}ds'ds - \frac{\mu_0 l}{4\pi}(1+\varepsilon_r) \quad (58)$$

and the radiation resistance of M subcircuits is

$$R^H_{mm} = 80\pi^2[(l/\lambda_0)^2 + \sqrt{\varepsilon_r}(l/\lambda_r)^2]. \quad (59)$$

It is obvious that the self-radiation resistances in both the E and M subcircuits are always greater than zero. However, the resistive coupling between the mth and kth ($m \neq k$) current cells is not necessarily positive in a passive system.

VII. Passivity of the Generalized PEEC Model

Passivity is a crucial property for circuit analysis in the time domain [18]. A passive system is not able to generate energy on its own under any condition [19], [20]. Similar to [19], define the current vector $[I]$ and potential vector $[\bar{\Phi}]$ as

$$[I] = \begin{bmatrix} I^E \\ I^H \end{bmatrix} \quad \text{and} \quad [\bar{\Phi}] = \begin{bmatrix} \bar{\Phi}^E \\ \bar{\Phi}^H \end{bmatrix}. \quad (60)$$

The generalized PEEC model is passive only if for arbitrary $[I]$ and $[\bar{\Phi}]$, the cumulative energy of the PEEC is nonnegative. To acquire the sufficient condition, cisoidal currents $[i(t)]$ and voltages $[\varphi(t)]$ are picked as follows:

$$[i(t)] = [I]e^{\mathrm{st}} \quad (61)$$

$$[\varphi(t)] = [\bar{\Phi}]e^{\mathrm{st}} \quad (62)$$

where $s = \sigma + j\omega$ and σ is an arbitrary positive real number. The instantaneous power $p(t)$ of the PEEC model is

$$\begin{aligned} p(t) &= \mathrm{Re}\left\{e^{s^*t}[I]^H\begin{bmatrix} sL^{EE}+R^E & sL^{EH}+K^E \\ sL^{HE}+K^H & sL^{HH}+R^H\end{bmatrix}[I]e^{\mathrm{st}}\right\} + \mathrm{Re}\left\{e^{s^*t}[\bar{\Phi}]^H\begin{bmatrix} sC^E & 0 \\ 0 & sC^H\end{bmatrix}[\bar{\Phi}]e^{\mathrm{st}}\right\} \\ &= \mathrm{Re}\left\{[I]^H\begin{bmatrix} sL^{EE}+R^E & sL^{EH}+K^E \\ sL^{HE}+K^H & sL^{HH}+R^H\end{bmatrix}[I]\right\}e^{2\sigma t} + \mathrm{Re}\left\{[\bar{\Phi}]^H\begin{bmatrix} sC^E & 0 \\ 0 & sC^H\end{bmatrix}[\bar{\Phi}]\right\}e^{2\sigma t} \end{aligned} \quad (63)$$

where $[I]^H$ and $[\bar{\Phi}]^H$ are the transpose conjugates of $[I]$ and $[\bar{\Phi}]$, respectively, and s^* is the conjugate of $[s]$. The cumulative energy $E(t)$ absorbed by the circuit up to time t becomes

$$\begin{aligned} E(t) &= \int_{-\infty}^{t} p(t)dt \\ &= \mathrm{Re}\left\{[I]^H\begin{bmatrix} sL^{EE}+R^E & sL^{EH}+K^E \\ sL^{HE}+K^H & sL^{HH}+R^H\end{bmatrix}[I]\right\}\frac{e^{2\sigma t}}{2\sigma} + \mathrm{Re}\left\{[\bar{\Phi}]^H\begin{bmatrix} sC^E & 0 \\ 0 & sC^H\end{bmatrix}[\bar{\Phi}]\right\}\frac{e^{2\sigma t}}{2\sigma}. \end{aligned} \quad (64)$$

The integral converges because of $\sigma > 0$. The passivity condition requires $E(t)$ to be nonnegative, implying the two terms on the RHS of (64) should be greater than zero for arbitrary s. As $\exp(2\sigma t)/(2\sigma) > 0$, the constraint for a passive system that $E(t) \geq 0$ is equivalent to the following conditions:

$$\mathrm{Re}\left\{[I]^H\begin{bmatrix} sL^{EE}+R^E & sL^{EH}+K^E \\ sL^{HE}+K^H & sL^{HH}+R^H\end{bmatrix}[I]\right\} \geq 0 \quad (65)$$

and

$$\mathrm{Re}\left\{[\bar{\Phi}]^H\begin{bmatrix} sC^E & 0 \\ 0 & sC^H\end{bmatrix}[\bar{\Phi}]\right\} \geq 0. \quad (66)$$

Since $[sL^{EE,HH}+R^{E,H}] = [sL^{EE,HH}+R^{E,H}]^T$, $[sL^{EH}+K^E] = -[sL^{HE}+K^H]^T$, and $[sC^{E,H}] = [sC^{E,H}]^T$,

all circuit elements are real, (65) and (66) can be written as

$$\begin{aligned}&\mathrm{Re}\left\{[I]^H\begin{bmatrix} sL^{EE}+R^E & sL^{EH}+K^E \\ sL^{HE}+K^H & sL^{HH}+R^H\end{bmatrix}[I]\right\}\\&\quad=\frac{1}{2}[I]^H\begin{bmatrix} R^E & j\omega L^{EH} \\ j\omega L^{HE} & R^H\end{bmatrix}[I]\\&\qquad+\frac{\sigma}{2}[I]^H\begin{bmatrix} L^{EE} & 0 \\ 0 & L^{HH}\end{bmatrix}[I]\\&\quad\geq 0 \end{aligned}\tag{67}$$

$$\begin{aligned}&\mathrm{Re}\left\{[\bar{\Phi}]^H\begin{bmatrix} sC^E & 0 \\ 0 & sC^H\end{bmatrix}[\bar{\Phi}]\right\}\\&\quad=\frac{\sigma}{2}[\bar{\Phi}]^H\begin{bmatrix} C^E & 0 \\ 0 & C^H\end{bmatrix}[\bar{\Phi}]\\&\quad\geq 0. \end{aligned}\tag{68}$$

In other words, the eigenvalues $[\lambda_L]$, $[\lambda_C]$, and $[\lambda_L^{\mathrm{Rad}}]$ of the three matrices on the RHS of (67) and (68) must be nonnegative, which are defined as

$$[\lambda_L]=\lambda\left\{\begin{bmatrix} L^{EE} & 0 \\ 0 & L^{HH}\end{bmatrix}\right\}\tag{69}$$

$$[\lambda_C]=\lambda\left\{\begin{bmatrix} C^E & 0 \\ 0 & C^E\end{bmatrix}\right\}\tag{70}$$

$$\left[\lambda_L^{\mathrm{Rad}}\right]=\lambda\left\{\begin{bmatrix} R^E & j\omega L^{EH} \\ j\omega L^{HE} & R^H\end{bmatrix}\right\}\tag{71}$$

where $[\lambda_L]$, $[\lambda_C]$ are the eigenvalues of the inductive and capacitive matrices, respectively; $[\lambda_L^{\mathrm{Rad}}]$ is the eigenvalue of element matrices that contribute to the radiation by current cells. The following NPV factor $\Delta F(\lambda)$, which is similar to that defined in [13], is used to quantify the degree of passivity violation:

$$\Delta F(\lambda)=\sqrt{\sum_{i=1}^{N}\Delta\lambda_i(\omega)^2}\Big/\sqrt{\sum_{i=1}^{N}\lambda_i(\omega)^2}\tag{72}$$

where $\Delta\lambda_i$ is constructed by

$$\Delta\lambda_i(\omega)=\begin{cases}0, & \lambda_i(\omega)\geq 0\\ -\lambda_i(\omega), & \lambda_i(\omega)<0\end{cases}\tag{73}$$

in which λ_i is the element of $[\lambda]$.

The range of ΔF is $[0, 1]$. Obviously, the closer the ΔF to 1, the severer the nonpassivity is. If ΔF equals zero, the circuit model is strictly passive. The second numerical example in Section VIII shows that the passivity of the generalized PEEC model is superior to that of the conventional S-PEEC model.

It should be mentioned that, as the circuit elements in the examples are evaluated numerically, the numerical error introduces very little nonpassivity as shown in Example C. Unlike conventional passivity enforcement methods [21]–[28], which are suitable to the state-space matrices, the amended system is not recoverable to the original circuit model. By observation, as long as the NPV factor is comparable to the numerical percentage error in the PEEC modeling, applying the passivity enforcement method introduced in [13] can remedy the minor nonpassivity without altering the circuit configuration.

The passivity enforcement is conducted by setting the negative-valued eigenvalues of an element matrix to very-small positive values, for example, one-tenth of the minimum positive eigenvalue. The concerned matrices can be reconstructed by multiplying the modified eigenvalues with the original eigenvectors.

When the NPV factor is reasonably small, the circuit responses before and after the enforcement show excellent agreement. On the other hand, the response of a conventional S-PEEC model shows a large error after the passivity enforcement due to the severe passivity violation, as shown in Example D.

For comparison purpose, the eigenvalues of circuit element matrices of the conventional complex LC S-PEEC model can be defined by the same principle as

$$[\lambda_L(\omega)]=\lambda\left\{\begin{bmatrix} \mathrm{Re}(M^E) & 0 \\ 0 & \mathrm{Re}(M^H)\end{bmatrix}\right\}\tag{74}$$

$$[\lambda_C(\omega)]=\lambda\left\{\begin{bmatrix} \mathrm{Re}(\tilde{C}^E) & 0 \\ 0 & \mathrm{Re}(\tilde{C}^H)\end{bmatrix}\right\}\tag{75}$$

$$\left[\lambda_L^{\mathrm{Rad}}(\omega)\right]=\lambda\left\{\begin{bmatrix} -\omega\mathrm{Im}(M^E) & j\mathrm{Im}(Z^E) \\ j\mathrm{Im}(Z^H) & -\omega\mathrm{Im}(M^H)\end{bmatrix}\right\}\tag{76}$$

$$\left[\lambda_C^{\mathrm{Rad}}(\omega)\right]=\lambda\left\{\begin{bmatrix} -\omega\mathrm{Im}(\tilde{C}^E) & 0 \\ 0 & -\omega\mathrm{Im}(\tilde{C}^H)\end{bmatrix}\right\}\tag{77}$$

where $[\lambda_L]$, $[\lambda_C]$ are the eigenvalues of the real part of inductive and capacitive matrices of the S-PEEC, respectively; $[\lambda_L^{\mathrm{Rad}}]$, $[\lambda_C^{\mathrm{Rad}}]$ are the eigenvalues of element matrices that contribute to the radiation by current and charge cells, respectively. The entries of $M^{E,H}$ and $Z^{E,H}$ are given in (24)–(27), and the capacitance matrices $\tilde{C}^{E,H}$ are the inverse matrices of complex potential coefficient matrices $P^{E,H}$ whose entries are defined in (28) and (29).

VIII. Numerical Examples

To validate the generalized PEEC model, four numerical examples are investigated.

A. LTCC Bandpass Filter

To demonstrate the ability of the PEEC to model problems whose electrical size is small, a low temperature co-fired ceramic (LTCC) filter module is investigated. This example concerns a six-layer LTCC bandpass filter shown in Fig. 7. The relative permittivity of the dielectric block is 7.8. The thickness of each layer is 91.44 μm. Three metal layers are printed on layers 1, 2, and 3 from the bottom ground layer. In the frequency range of interest, conductors are assumed to be infinitely thin and lossless. The conductor patches embedded inside the dielectric block are divided into 865 triangular cells and the dielectric surface including the ground plane introduces 796 triangular cells. Two delta-gap voltage sources are applied at the ports. The PEEC model contains 2742 branches and 1885 nodes and is analyzed using MNA [17]. The magnitude of the S-parameters by the proposed PEEC model and Agilent ADS commercial software (RF momentum module) are shown in Fig. 8. Good agreement is observed.

B. Rectangular Dielectric Resonator Antenna

A wide-band DRA whose dielectric resonances at higher order modes are taken into account is discussed to show

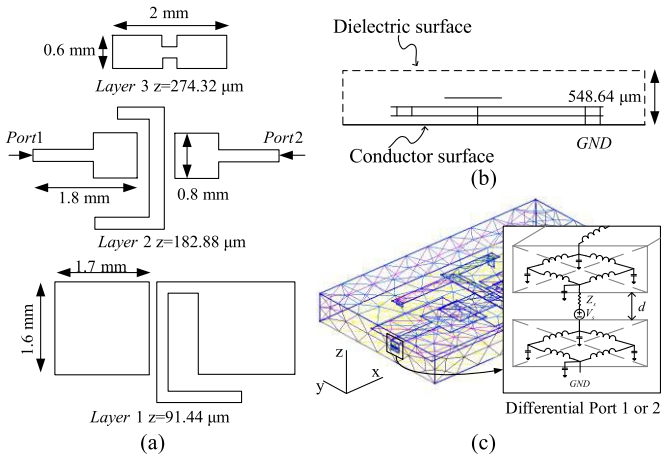

Fig. 7. LTCC bandpass filter. (a) Top view of each metal layer in the *xy* plane and its physical dimensions. (b) Side view of the filter in the *yz* plane. (c) Meshing scheme with port enlarged to illustrate the excitation method.

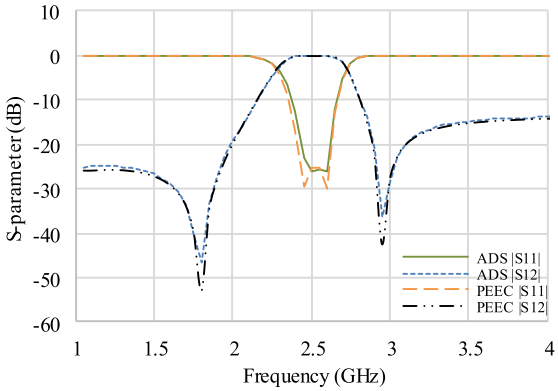

Fig. 8. S-parameter magnitude of the LTCC bandpass filter obtained by the generalized PEEC model and ADS results.

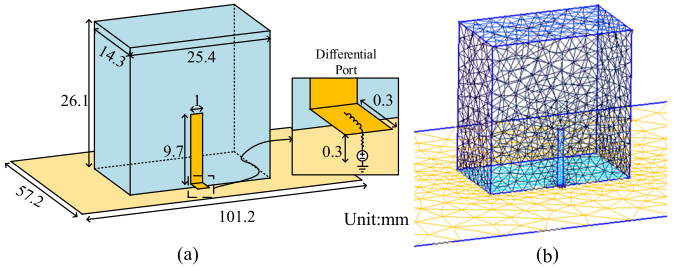

Fig. 9. Wide-band rectangular DRA. (a) Physical dimensions. (b) Meshing scheme.

the accuracy of the generalized PEEC in a wide frequency range. The physical dimensions and mesh scheme are shown in Fig. 9(a) and (b), respectively. A rectangular dielectric resonator with a relative permittivity of 9.8 is placed on a ground plane of finite size and is excited by a monopole antenna placed beside the dielectric resonator. A delta-gap voltage source is applied to a small segment of air-filled transmission lines away from the dielectric. In this example, a 0.3-mm-length and 0.3-mm-width conductor patch is attached to the bottom of the conductor, as shown in Fig. 9(a). The input impedance calculated by the PEEC model is compared

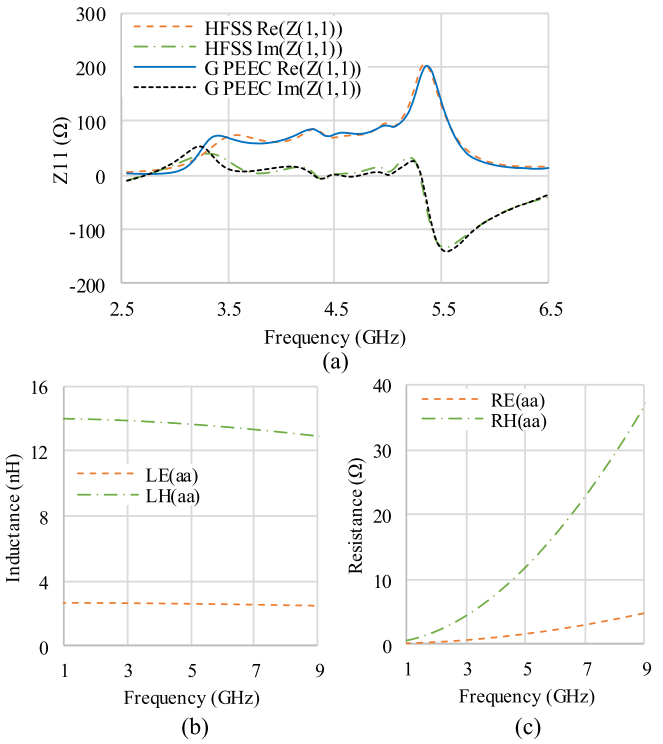

Fig. 10. (a) Input impedance (Z_{11}) obtained by the generalized PEEC model and HFSS. (b) Self-inductance of the electric and magnetic subcircuits. (c) Self-resistance of the electric and magnetic subcircuits.

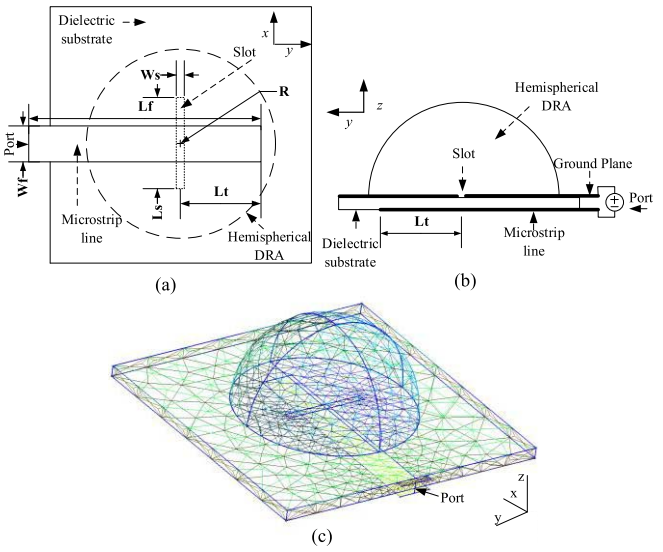

Fig. 11. Hemisphere DRA with a finite-sized substrate. (a) Bottom view in the *xy* plane. (b) Side view in the *yz* plane. (c) Meshing schemes.

with that by HFSS, as shown in Fig. 10(a). Fig. 10(b) and (c) shows the self-inductance and self-resistance of current cells in electric and magnetic subcircuits. Within the frequency range of interest, self-terms retain positive.

C. Hemispheric Dielectric Resonator Antenna

The third example is a microstrip line-fed slot-coupled hemisphere DRA, as depicted in Fig. 11. The radius *R*,

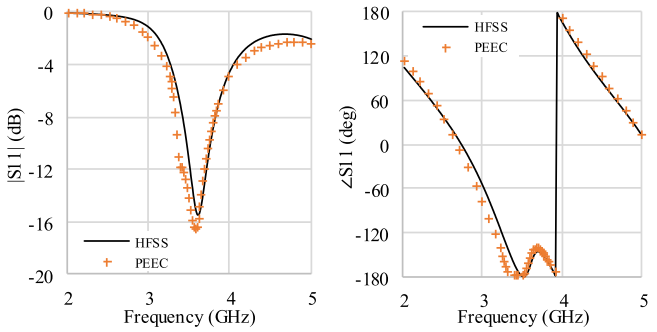

Fig. 12. Return loss (S_{11}) obtained by the proposed PEEC model and HFSS.

TABLE I
MAXIMUM $\Delta F(\lambda)$ IN FREQUENCY RANGE OF 0–5 GHz

Testing eigenvalues	Conventional S-PEEC	Generalized PEEC
Inductances (λ_L)	1.62×10^{-2}	1.75×10^{-3}
Capacitances (λ_C)	0	0
Resistances (λ_{Rad})	1.00	9.43×10^{-4}

slot width W_s, slot length L_s, feeding microstrip linewidth W_f, and length L_f are 12.5, 1, 12, 4.7, and 33.63 mm, respectively. This example consists of two dielectric blocks with different relative permittivities. One is the microstrip line substrate with a thickness of 1.57 mm and a dielectric constant of 2.33. The other dielectric block is the dielectric resonator whose dielectric constant is 9.5. As shown in Fig. 11(c), the triangular meshes accordingly fit the hemispheric structure well. The computed return losses using the proposed PEEC model and that by HFSS are superimposed in Fig. 12. A good correlation can be observed.

The NPV factors ΔF of the generalized PEEC model and the conventional S-PEEC model are examined in the frequency range of 0–5 GHz. The maximum $\Delta F(\lambda)$ is listed in Table I. It can be noticed that: 1) the capacitance matrices of both the S-PEEC model and generalized PEEC model are all semipositive definite; 2) little passivity violation appears in the inductive matrix in both PEEC models; and 3) the radiation resistance matrices of the S-PEEC model show a strong passivity violation, whereas the generalized PEEC model preserves good passivity. The NPV factors of the generalized PEEC and S-PEEC model are superimposed in Fig. 13. The NPV factors of the radiation resistance matrix of the generalized PEEC are below 0.01, whereas $\Delta F(\lambda_c^{\mathrm{Rad}})$ of the S-PEEC model is 1 over the frequency band, which means that the radiation resistance associated with capacitive branches suffers from severe nonpassivity in the conventional S-PEEC model. The minor nonpassivity (less than 0.2%) in the proposed PEEC model is introduced by the numerical error in evaluating the circuit elements. The passivity enforcement method introduced in [13] can be applied to compensate the inaccuracy.

D. Patch Antenna With Finite Substrate

The last example is a patch antenna with a finite dielectric substrate. The structure and physical dimensions are illustrated

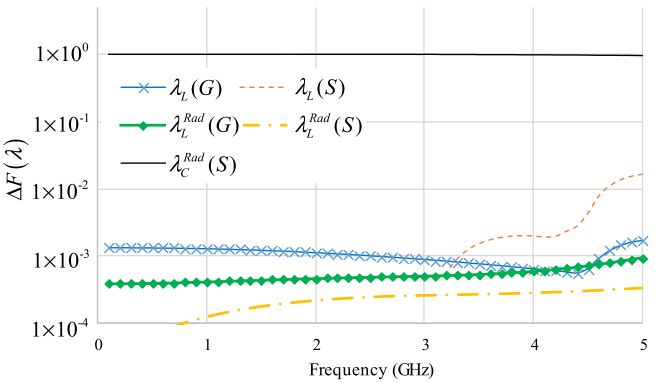

Fig. 13. NPV factor ΔF of the conventional S-PEEC (S) and the generalized PEEC (G).

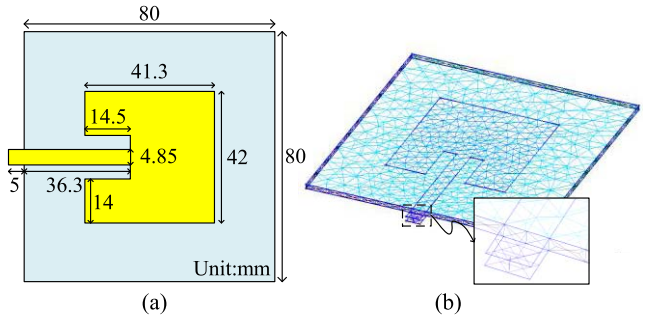

Fig. 14. (a) Physical dimensions of the patch antenna. (b) Meshing scheme of the patch antenna.

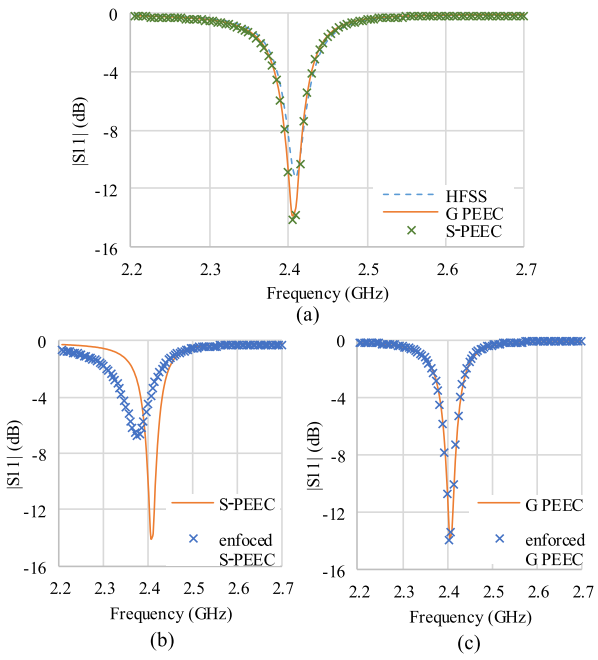

Fig. 15. (a) Magnitude of return loss (S_{11}) obtained by HFSS, the proposed PEEC model, and the S-PEEC model. (b) $|S_{11}|$ of the generalized PEEC model before and after passivity enforcement. (c) $|S_{11}|$ of the S-PEEC model before and after passivity enforcement.

in Fig. 14(a) and (b). The relative permittivity of the substrate is 2.2. As shown in Fig. 14(a), a small section of the transmission line is added to ensure the excitation away from the

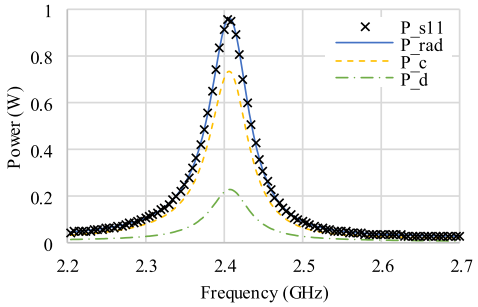

Fig. 16. Distributive power and the total radiated power calculated from S_{11}.

surface of the dielectric substrate. The thickness of the substrate is 1.585 mm. The conductors are 0.1 mm thick and lossless. The return loss calculated by the generalized PEEC and conventional S-PEEC agrees with that of HFSS well, as shown in Fig. 15(a). After applying the passivity enforcement to the circuit of the generalized PEEC and S-PEEC, the generalized PEEC shows better accuracy as shown in Fig. 15(b) and (c). Assuming the total input power is 1 W, the distributive power defined in (50) is verified by comparing the total power consumed by the resistors and coupling (*P_rad*) with the total radiated power calculated from S-parameters (*P_s11*). The summation of the distributive radiated power matches well with *P_s11* as shown in Fig. 16. The power consumed on the proposed PEEC related to conductors (*P_c*) and dielectrics (*P_d*) is also shown in Fig. 16. The computation time of the generalized PEEC model and that of the S-PEEC model without passivity enforcement are 26 min 23 s and 24 min 2 s, respectively.

IX. Conclusion

In this article, a generalized PEEC model for EM problems, involving metals and piecewise homogeneous dielectrics of finite size, is introduced. With the static potential coefficients and generalized complex inductance, the PEEC model can accurately describe the radiation effect while maintaining the passivity of the circuit model. The triangular mesh scheme is used for fittingly discretizing highly irregular-shaped objects. The radiation effect of the subcircuit for a dielectric block is also accurately incorporated into the proposed PEEC model. The superiority of the passivity of the proposed PEEC model is demonstrated by checking the NPV factors of the circuit element matrices with those of the existing S-PEEC model. Four practical numerical examples are given to demonstrate the effectiveness and validation of the proposed PEEC model. It is expected that the generalized PEEC model can provide a unique means to convert a general EM problem into a circuit model with superior passivity property. It should be mentioned that the generalized PEEC model is not suitable for modeling the problems that involve highly inhomogeneous dielectrics. For an electrically large problem, an appropriate model order reduction method, or a micromodeling circuit, for the PEEC model needs to be developed.

References

[1] A. E. Ruehli and A. C. Cangellaris, "Progress in the methodologies for the electrical modeling of interconnects and electronic packages," *Proc. IEEE*, vol. 89, no. 5, pp. 740–771, May 2001.

[2] R. F. Harrington, *Field Computation by Moment Methods*, 1st ed. New York, NY, USA: Macmillan, 1968, pp. 189–191.

[3] J. M. Jin, *The Finite Element Method in Electromagnetics*, 2nd ed. New York, NY, USA: Wiley, 2002.

[4] A. Taflove and S. C. Hagness, *Computational Electrodynamics: The Finite-Difference Time-Domain Method*. Norwood, MA, USA: Artech House, 2005.

[5] H. Heeb and A. E. Ruehli, "Three-dimensional interconnect analysis using partial element equivalent circuits," *IEEE Trans. Circuits Syst. I, Fundam. Theory Appl.*, vol. 39, no. 11, pp. 974–982, Nov. 1992.

[6] A. E. Ruehli and H. Heeb, "Circuit models for three-dimensional geometries including dielectrics," *IEEE Trans. Microw. Theory Tech.*, vol. 40, no. 7, pp. 1507–1516, Jul. 1992.

[7] D. Gope, A. E. Ruehli, C. Yang, and V. Jandhyala, "(S)PEEC: Time- and frequency-domain surface formulation for modeling conductors and dielectrics in combined circuit electromagnetic simulations," *IEEE Trans. Microw. Theory Tech.*, vol. 54, no. 6, pp. 2453–2464, Jun. 2006.

[8] Y. Dou and K.-L. Wu, "Direct mesh-based model order reduction of PEEC model for quasi-static circuit problems," *IEEE Trans. Microw. Theory Tech.*, vol. 64, no. 8, pp. 2409–2422, Aug. 2016.

[9] L. K. Yeung and K.-L. Wu, "Generalized partial element equivalent circuit (PEEC) modeling with radiation effect," *IEEE Trans. Microw. Theory Tech.*, vol. 59, no. 10, pp. 2377–2384, Oct. 2011.

[10] L. K. Yeung and K.-L. Wu, "PEEC modeling of radiation problems for microstrip structures," *IEEE Trans. Antennas Propag.*, vol. 61, no. 7, pp. 3648–3655, Jul. 2013.

[11] Y. S. Cao, L. J. Jiang, and A. E. Ruehli, "Distributive radiation and transfer characterization based on the PEEC method," *IEEE Trans. Electromagn. Compat.*, vol. 57, no. 4, pp. 734–742, Aug. 2015.

[12] C.-C. Chou, W.-C. Lee, and T.-L. Wu, "A rigorous proof on the radiation resistance in generalized PEEC model," *IEEE Trans. Microw. Theory Tech.*, vol. 64, no. 12, pp. 4091–4097, Dec. 2016.

[13] Y. Dou and K.-L. Wu, "A passive PEEC-based micromodeling circuit for high-speed interconnection problems," *IEEE Trans. Microw. Theory Tech.*, vol. 66, no. 3, pp. 1201–1214, Mar. 2018.

[14] L. Lombardi, G. Antonini, and A. E. Ruehli, "Analytical evaluation of partial elements using a retarded Taylor series expansion of the Green's function," *IEEE Trans. Microw. Theory Tech.*, vol. 66, no. 5, pp. 2116–2127, May 2018.

[15] Y. Dou, L.-K. Yeung, and K.-L. Wu, "Time-domain analysis of circuits with frequency-dependent elements using a SPICE-like solver," in *Proc. IEEE Elect. Design Adv. Packag. Syst. Symp. (EDAPS)*, Nara, Japan, Dec. 2013, pp. 193–196.

[16] S. Rao, D. Wilton, and A. Glisson, "Electromagnetic scattering by surfaces of arbitrary shape," *IEEE Trans. Antennas Propag.*, vol. AP-30, no. 3, pp. 409–418, May 1982.

[17] C.-W. Ho, A. E. Ruehli, and P. A. Brennan, "The modified nodal approach to network analysis," *IEEE Trans. Circuits Syst.*, vol. CAS-22, no. 6, pp. 504–509, Jun. 1975.

[18] P. Triverio, S. Grivet-Talocia, M. S. Nakhla, F. G. Canavero, and R. Achar, "Stability, causality, and passivity in electrical interconnect models," *IEEE Trans. Adv. Packag.*, vol. 30, no. 4, pp. 795–808, Nov. 2007.

[19] S. Grivet-Talocia and B. Gustavsen, *Passive Macromodeling: Theory and Applications*, 1st ed. Hoboken, NJ, USA: Wiley, 2016, pp. 6–13.

[20] G. H. Golub and C. F. van Loan, "Positive definite system," in *Matrix Computation*, 4th ed. Baltimore, MD, USA: The Johns Hopkins Univ. Press, 2013, p. 160.

[21] R. N. Shorten, P. Curran, K. Wulff, and E. Zeheb, "A note on spectral conditions for positive realness of transfer function matrices," *IEEE Trans. Autom. Control*, vol. 53, no. 5, pp. 1258–1261, Jun. 2008.

[22] S. Boyd, V. Balakrishnan, and P. Kabamba, "A bisection method for computing the H_∞ norm of a transfer matrix and related problems," *Math. Control Signals Syst.*, vol. 2, no. 1, pp. 207–219, Jan. 1989.

[23] S. Grivet-Talocia, "Passivity enforcement via perturbation of Hamiltonian matrices," *IEEE Trans. Circuits Syst. I, Reg. Papers*, vol. 51, no. 9, pp. 1755–1769, Sep. 2004.

[24] Z. Bai and R. W. Freund, "Eigenvalue-based characterization and test for positive realness of scalar transfer functions," *IEEE Trans. Autom. Control*, vol. 45, no. 12, pp. 2396–2402, Dec. 2000.

[25] C. Schroeder and T. Stykel, *Passivity Check in Passivation of LTI Systems*, document TR-368-2007, 2007.

[26] B. Gustavsen and A. Semlyen, "Enforcing passivity for admittance matrices approximated by rational functions," *IEEE Trans. Power Syst.*, vol. 16, no. 1, pp. 97–104, Feb. 2001.

[27] W. D. C. Boaventura, A. Semlyen, M. R. Iravani, and A. Lopes, "Sparse network equivalent based on time-domain fitting," *IEEE Trans. Power Del.*, vol. 17, no. 1, pp. 182–189, Jan. 2002.
[28] A. Lamecki and M. Mrozowski, "Equivalent SPICE circuits with guaranteed passivity from nonpassive models," *IEEE Trans. Microw. Theory Tech.*, vol. 55, no. 3, pp. 526–532, Mar. 2007.

Yang Jiang received the B.S. degree in electronics engineering from The Chinese University of Hong Kong, Hong Kong, in 2013, where he is currently pursuing the Ph.D. degree.

His current research interests include partial element equivalent circuit (PEEC) modeling, full-wave circuit domain modeling for signal integrity and electromagnetic compatibility problems, and compact PEEC models for electromagnetic problems including inhomogeneous dielectrics in both the frequency and time domains.

Yuhang Dou (S'13) received the B.S. degree in electronic engineering from the Nanjing University of Science and Technology, Nanjing, China, in 2012. She is currently pursuing the Ph.D. degree at The Chinese University of Hong Kong, Hong Kong.

Her current research interests include physics-based circuit-domain modeling methods for radiation problems and signal integrity (SI) analysis of high-speed large-scale interconnection and packaging problems.

Dr. Dou was a recipient of the Fist Runner Up Awards in both 2015 and 2018 IEEE Hong Kong AP/MTT Postgraduate Conferences.

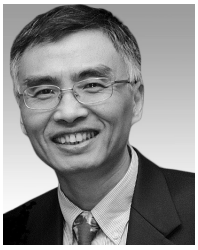

Ke-Li Wu (M'90–SM'96–F'11) received the B.S. and M.Eng. degrees from the Nanjing University of Science and Technology, Nanjing, China, in 1982 and 1985, respectively, and the Ph.D. degree from Laval University, Quebec, QC, Canada, in 1989.

From 1989 to 1993, he was a Research Engineer with McMaster University, Hamilton, ON, Canada. In 1993, he joined the Corporate Research and Development Division, Honeywell Aerospace, Cambridge, ON, Canada, where he was a Principal Member of Technical Staff. Since 1999, he has been with The Chinese University of Hong Kong, Hong Kong, where he is currently a Professor and the Director of the Radiofrequency Radiation Research Laboratory. His current research interests include EM-based circuit domain modeling of high-speed interconnections, robot automatic tuning of microwave filters, decoupling techniques of MIMO antennas, and the Internet of Things technologies.

Dr. Wu is a member of the IEEE MTT-8 Subcommittee. He serves as a TPC member for many prestigious international conferences. He was a recipient of the 1998 COM DEV Achievement Award and the Asia–Pacific Microwave Conference Prize twice in 2008 and 2012, respectively. He was an Associate Editor of the IEEE TRANSACTIONS ON MICROWAVE THEORY AND TECHNIQUES from 2006 to 2009.